



The influence of sac centreline on saccular aneurysm rupture: computational study

Downloaded from: <https://research.chalmers.se>, 2023-09-08 04:52 UTC

Citation for the original published paper (version of record):

Jiang, H., Lu, Z., Barzegar Gerdroodbary, M. et al (2023). The influence of sac centreline on saccular aneurysm rupture: computational study. *Scientific Reports*, 13(1): 11288-.
<http://dx.doi.org/10.1038/s41598-023-38466-2>

N.B. When citing this work, cite the original published paper.



OPEN The influence of sac centreline on saccular aneurysm rupture: computational study

Hao Jiang¹, Zhiwei Lu^{2✉}, M. Barzegar Gerdroodbary^{3✉}, Amir Sabernaemi⁴ & Sajad Salavatidezfouli⁵

The geometric characteristics of a saccular aneurysm play a crucial role in its rupturing. This article thoroughly investigates the impact of the sac centerline on aneurysm rupture, with a focus on identifying significant factors related to rupture at different time intervals. The study employs comprehensive computational simulations of six models of the ICA with varying coiling porosities and blood HCTs, using CFD analysis to examine WSS, OSI, pressure, and velocity within the saccular aneurysm for different sac centerlines. The results indicate that higher blood HCT levels lead to increased WSS and pressure values on the aneurysm wall, while OSI and mean velocity decrease. The study also reveals that coiling techniques can significantly reduce the risk of rupture, as decreasing coil porosity (increasing coil permeability) increases OSI and pressure while decreasing WSS and blood velocity within the aneurysm sac.

Intracranial aneurysms (IAs) refer to the central dilatation of vessel walls, which commonly occur along the branches of the Circle of Willis. These cerebrovascular disorders carry a high risk of mortality and morbidity upon aneurysm rupture, with approximately 45% of cases resulting in permanent disability or death and possible damage to surrounding cerebral tissues. The prevalence of IAs in the adult population is estimated to be around 5–9%. However, with advances in medical imaging technology over the last three decades, more than 50% of cerebral aneurysms are now detected before rupture occurs. This has provided researchers with access to valuable data and information about the geometric characteristics of aneurysms, which is essential for selecting appropriate treatments^{1–3}.

Previous studies^{4,5} have made extensive efforts to highlight the significant role of CFD in the detection and treatment of this disorder. Most of these studies have confirmed the importance of wall shear stress in the initiation stage due to its impact on the endothelial layer^{6,7}. This layer is capable of converting mechanical signals into biological signals and activating biochemical pathways within the vessel wall.

The orientation and structure of the endothelial cells are altered when flow conditions deviated from normal status^{8,9}. Consequently, a damaging remodeling of the vessel wall occurs over the above-mentioned events. The precise character of the hemodynamics is not completely preserved, but, extensively recognized research done by sadeh et al.¹⁰ indicates that an abnormal hemodynamical situation including high WSSG and WSS initiates the negative reorientation and reshaping of the endothelial monolayer and plane muscle cells^{11,12}. Besides, this layer under disturbed flow conditions is known to exhibit several pathological features^{13,14}.

Coiling embolism is a popular technique for treating saccular aneurysms^{15,16}. The effectiveness of this method in reducing the risk of aneurysm rupture depends on its impact on the hemodynamics of different aneurysms^{17,18}. By applying CFD to simulate blood flow within the ICA with coiling embolism, the hemodynamic aspects of coiling can be revealed, and the required percentage of coil for risk reduction of aneurysm rupture can be determined^{14,16}. However, due to the complexity and diversity of aneurysm shapes and geometries, reliable research on this topic requires real 3-D geometries of aneurysms⁵. In this study, six different ICA shapes were chosen to investigate the effect of aneurysm shape on the efficiency of coiling. Blood flow analysis was also performed on these models to examine their hemodynamic characteristics.

¹Dept. Neurosurg, Shulan (Hangzhou) Hospital Affiliated to Zhejiang Shuren University Shulan International Medical College, Hangzhou 310000, Zhejiang, China. ²Hangzhou Heyunjia Hospital, Hangzhou 310000, Zhejiang, China. ³Department of Mechanical Engineering, Babol Noshirvani University of Technology, Babol, Iran. ⁴Department of Space, Earth and Environment, Chalmers University of Technology, Gothenburg, Sweden. ⁵Mathematics Area, MathLab, International School for Advanced Studies (SISSA), Trieste, Italy. ✉email: luzhiwei1316@163.com; mbarzegar@yahoo.com

This study aims to investigate the evolving flow characteristics within reassembled pre-aneurysmal shapes by analyzing local flow pathways. Computational fluid dynamics (CFD) is used to simulate blood flow within cerebral aneurysms. The study identifies a primary and secondary flow pathway based on the orientation of the sac and vessel centerlines. Six different internal carotid aneurysms (ICAs) are analyzed to determine the main effects of blood hematocrit and coiling embolism on wall shear stress (WSS) and oscillatory shear index (OSI) values.

Material and methods

It is confirming that all methods were carried out in accordance with relevant guidelines and regulations. Besides, all experimental protocols were approved by of the Ca' Granda Niguarda Hospital and it is confirmed that informed consent was obtained from all subjects and/or their legal guardian(s).

As previously mentioned, real 3-dimensional models of the ICA are crucial for investigating the impact of blood on aneurysm rupture when coiling embolism is applied. For this study, we selected six ICA models from Aneurisk¹⁹ for our simulations. Given the importance of this factor on aneurysm rupture, we aimed to examine and compare the distribution of wall shear stress (WSS), oscillatory shear index (OSI), and pressure on the six selected models. The geometric details of the aneurysms chosen for analysis are presented in Table 1, and their geometrical features are nearly identical (Fig. 1). All selected cases, except for Model B, are unruptured models.

Model	Sac Volume	Sac Centerline Length	WSS Min Sac (pa)	OSI Max Sac	Mean Wall Pressure (Pa)	Max Wall Pressure (Pa)	Mean Sac Pressure (Pa)	Max Sac Pressure (Pa)	OSI Mean Sac	Mean Vel Sac m/s	Max Vel Sac m/s	MVA_Int m/s
A	30.80887	3.478118	1.224985	0.162072	24502.37	24577.9	24486.24	24579.01	0.00588	0.188099	0.57415	0.279609
B	68.82005	5.762182	0.861677	0.207146	18061.55	18213.61	17987.76	18216.28	0.006905	0.43264	0.983588	0.697393
C	125.2596	6.510948	0.307939	0.31419	19191.12	19830.16	19132.63	19838.42	0.00776	0.366304	1.223228	
D	289.3767	8.308456	0.230072	0.375356	19423.67	20180.7	19328.86	20189.18	0.013998	0.509628	1.756638	0.661451
E	533.6227	10.65323	0.108216	0.383909	19213.4	19376.57	19194.86	19377.64	0.008466	0.173294	0.907829	0.429496
F	1312.026	15.31556	0.002808	0.478797	17,505.05	17,689.06	17,507.37	17,678.75	0.058676	0.026245	1.649474	0.396914

Table 1. Details of selected ICA aneurysm.

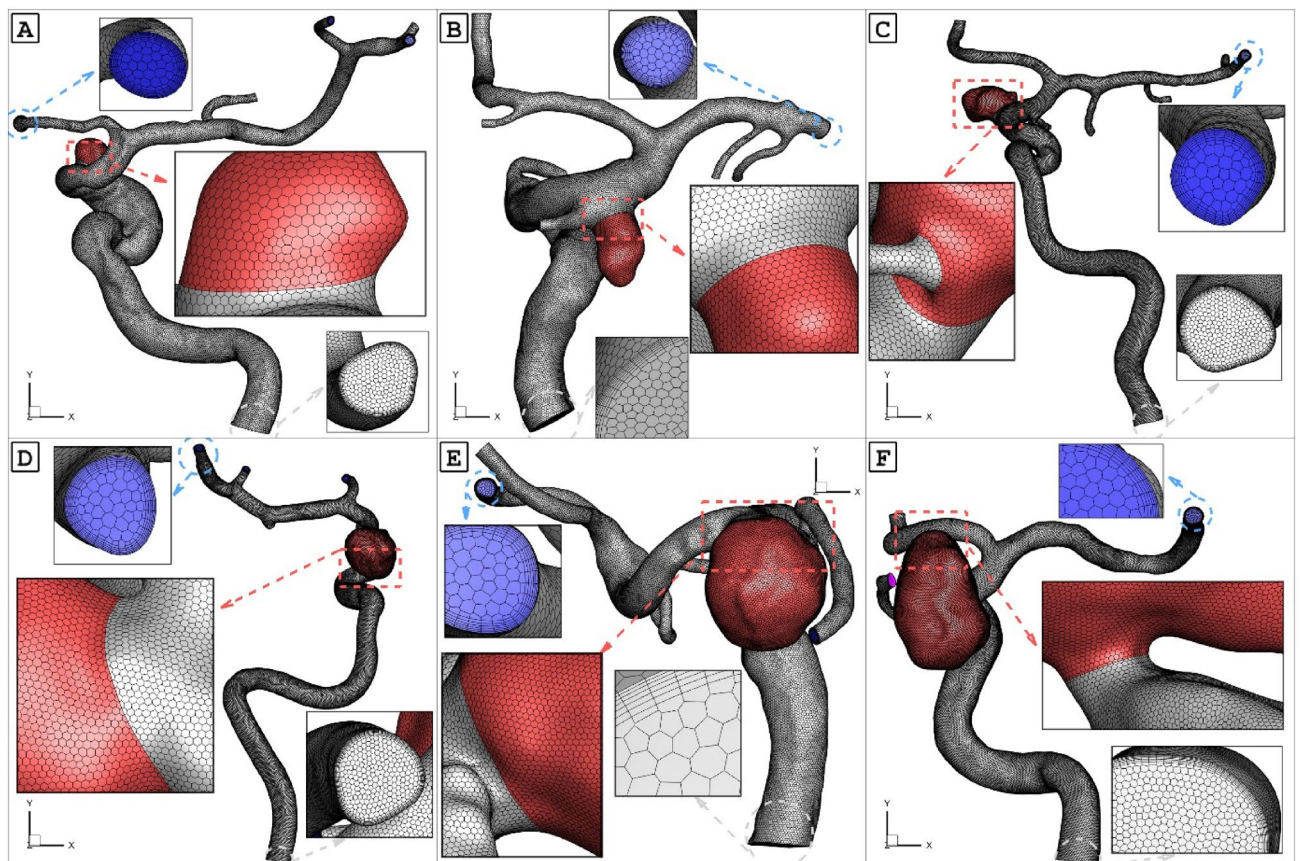


Figure 1. six cases with applied grids.

For the computational study of blood flow through cerebral aneurysms, the unsteady Navier–Stokes equations are typically solved, and blood flow is considered non-Newtonian. In this study, a commercial software called ANSYS, which is commonly used for engineering and biomedical modeling^{20–25}, was used for CFD simulations. The carotid vessel walls and bloodstream were modeled along the axial direction using either fully coupled or one-way fluid–structure interaction (FSI) simulations. In the one-way FSI simulation, the fluid model was solved first, and the pressure obtained was transferred to the solid domain of the wall as an exterior loading for estimating the structural stress, without any additional interaction between the solid and fluid domains. In contrast, the fully coupled FSI simulation used non-linear incremental iterative procedures for interaction between the two domains. In this study, the one-way FSI procedure was applied for simulating blood flow inside the aneurysm.

The Casson model was used to estimate the viscosity of blood rheology²⁶. Three cardiac cycles were investigated due to the unsteady characteristics of blood flow (Fig. 2), and the results of the last cycle were selected to ensure that the results were not dependent on initial transients^{27,28}. The inlet and outlet were positioned far enough from the aneurysm sac to enable the velocity profile to progress appropriately. The inlet blood flow was applied via mass flow rate, while the outlet was a pressure outlet. The reported value in this study is for the peak systolic condition, which is of particular importance^{29–31}.

Results and discussion

Blood viscosity effects. Due to the importance of the blood HCT on hemodynamics, four different HCTs are examined on a specific model of D which has a mean sac centreline among selected models. Table 2 presents the impacts of various HCTs on the blood characteristics at peak systolic.

The influence of HCT on the mean WSS on the selected aneurysm (model D) is demonstrated in Figs. 3 and 4. It is found that increasing the HCT directly raises the mean WSS on the chosen aneurysm. Figure 4 also confirms that the maximum value of WSS happens nearby the ostium section and it increased by rising the HCT.

The Fig. 5 plots the impacts of HCT on the OSI values at peak systolic instant. It is observed that the value of mean HCT decreases about 60% with 40% increase of HCT. Figure 6 also displays the variation of the OSI on the aneurysm wall and the variation of the OSI indicate that a high value of OSI occurs near the dome section.

The Figs. 7 and 8 demonstrate the impacts of the HCT on the mean pressure distribution on the aneurysm wall at peak systolic time instant. Since increasing the HCT results in high viscosity, the pressure on the aneurysm wall significantly increases and the high-pressure region happens exactly on the dome of the aneurysm as displayed in Fig. 8. In fact, the pressure distribution is the main reason for deformation and shape of the aneurysm.

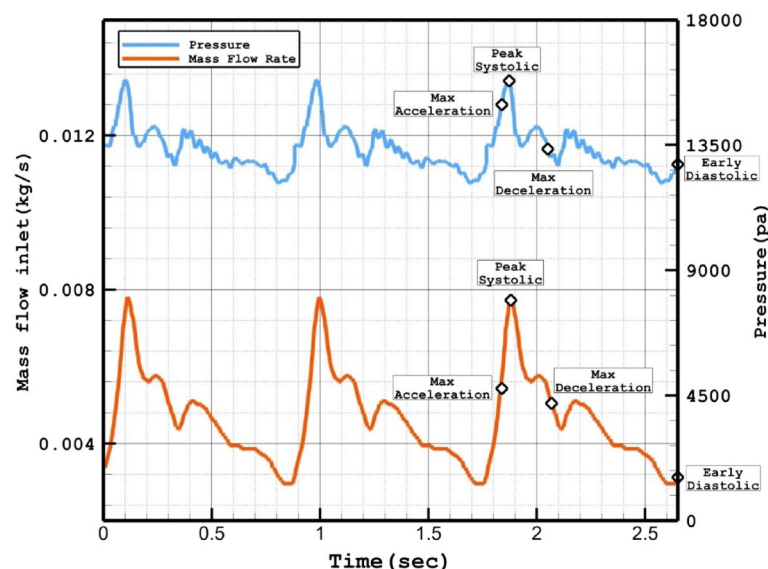


Figure 2. Applied mass flow rate and pressure profile at inlet and outlets¹.

HCT	WSS Max Sac (pa)	WSS Mean Sac (pa)	WSS Min Sac (pa)	OSI Max Sac	OSI Mean Sac	MWA_Vel_interior (m/s)	Sac mean pressure (pa)	Sac mean Velocity (m/s)
0.33	140.5824	17.0533	0.287034	0.417075	0.024434	1.016822	19,136.06	0.524941
0.4	147.6993	18.39566	0.230072	0.375356	0.013998	0.987321	19,328.86	0.509628
0.45	152.1064	19.258	0.233781	0.330751	0.009701	0.974953	19,551.4	0.498876
0.5	157.6807	19.8118	0.368156	0.341078	0.007257	0.954	19,875.23	0.48059

Table 2. Details of obtained results on selected model (D) for different HCTs.

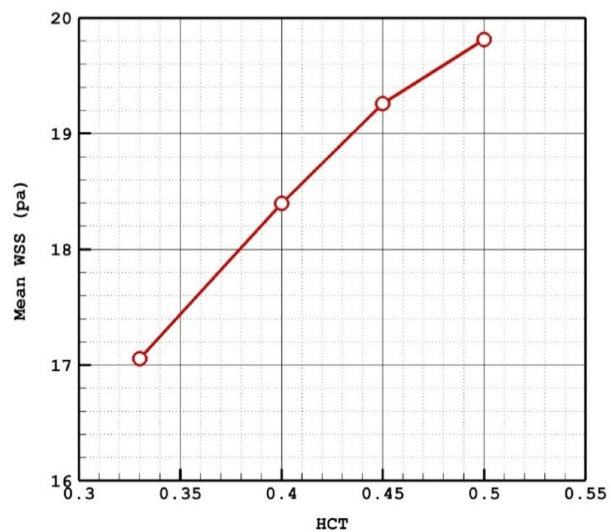


Figure 3. HCT effects on mean WSS.

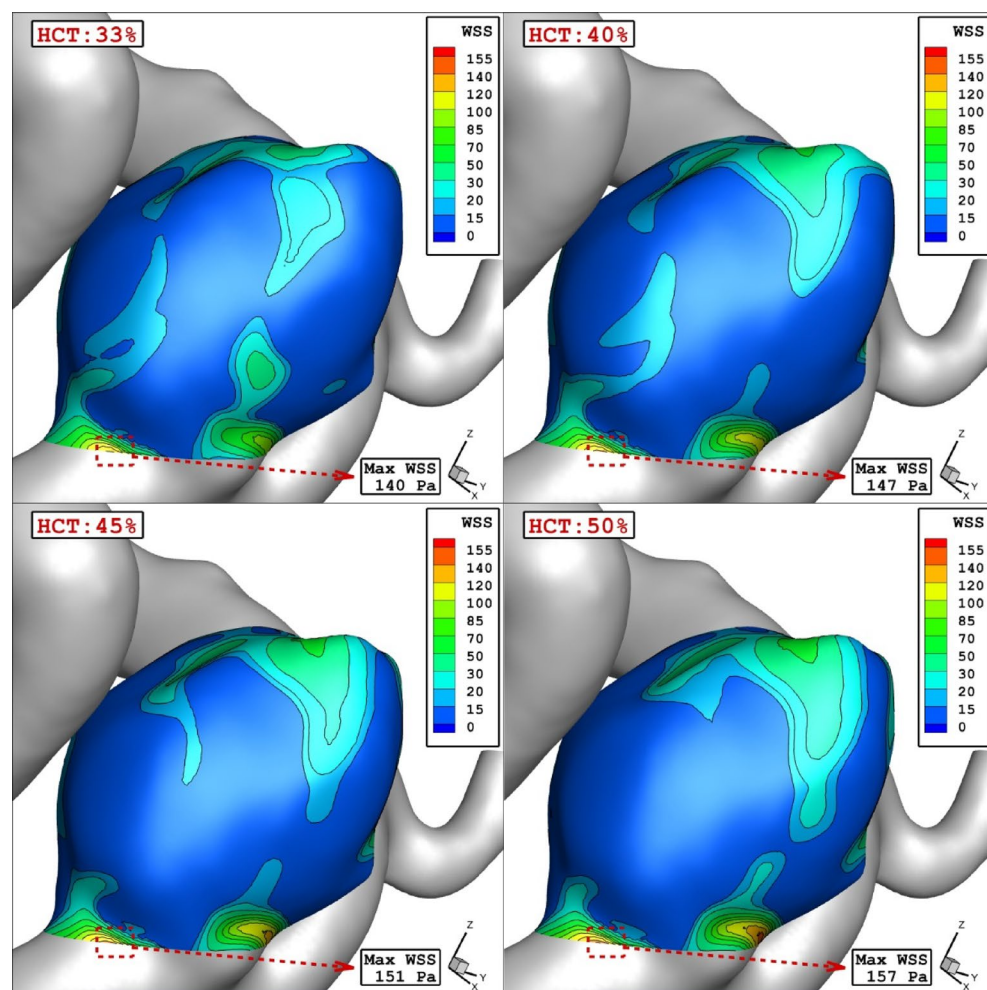


Figure 4. WSS contours in different HCTs.

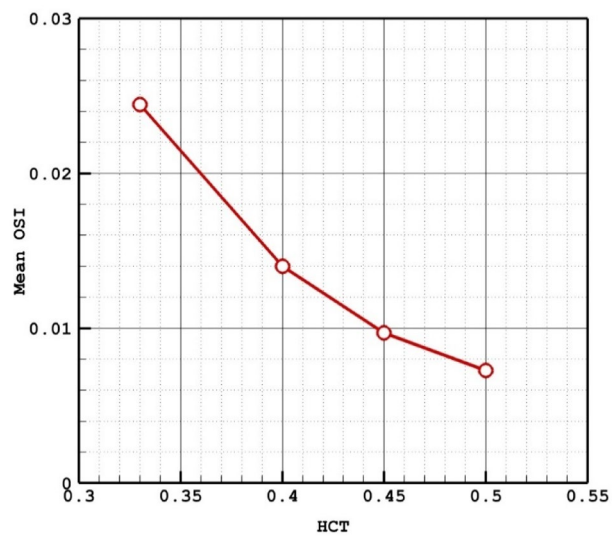


Figure 5. HCT effects on mean OSI.

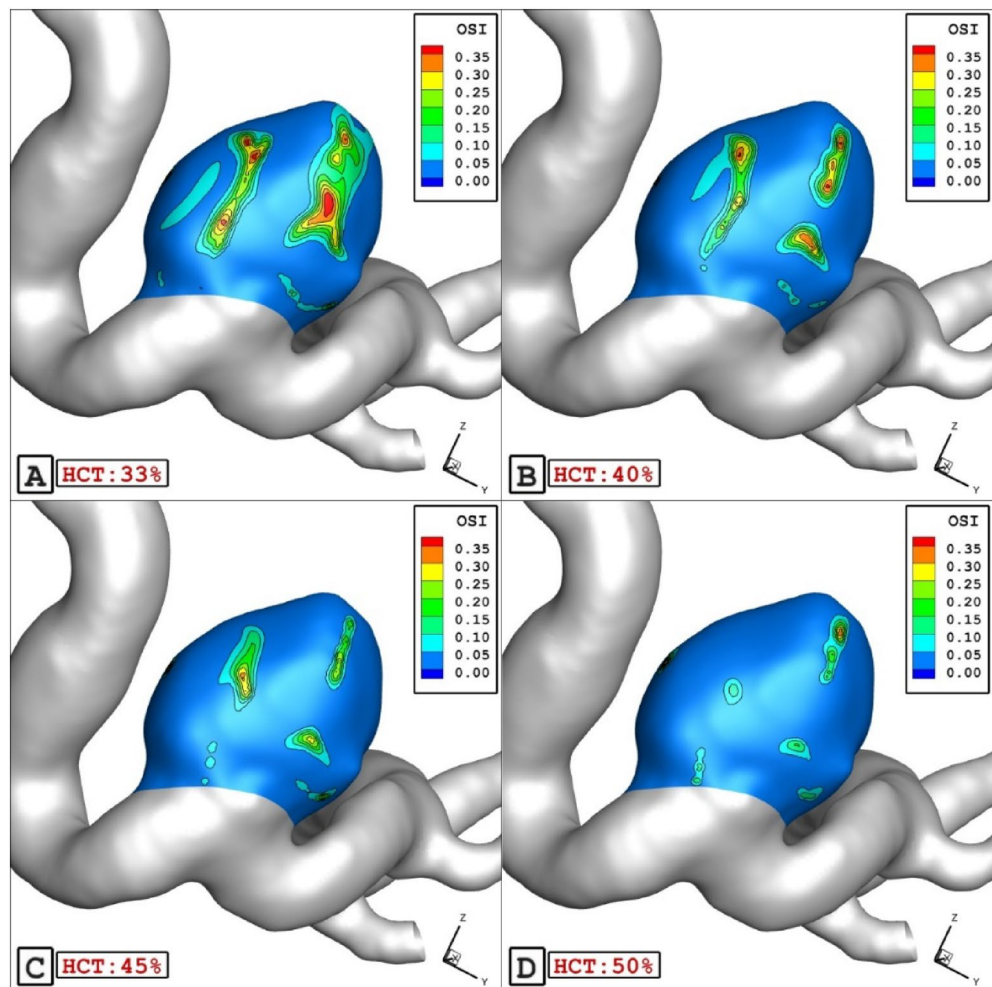


Figure 6. OSI contours in different HCTs.

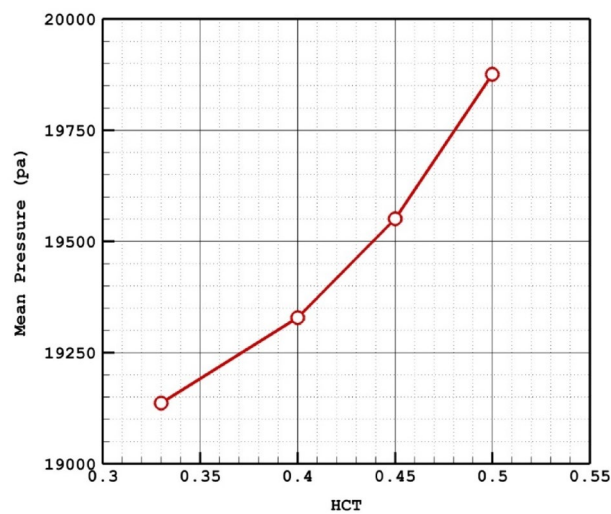


Figure 7. HCT effects on mean sac wall pressure.

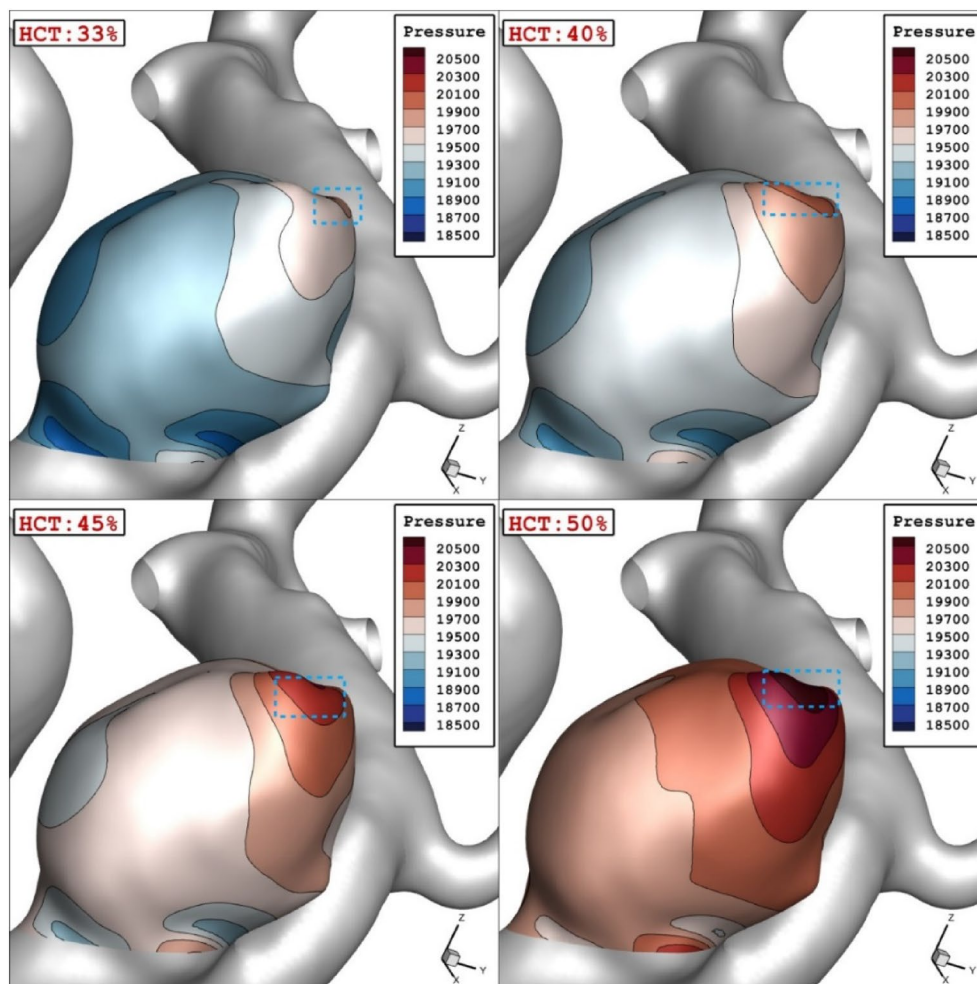


Figure 8. Wall Pressure contours in different HCTs.

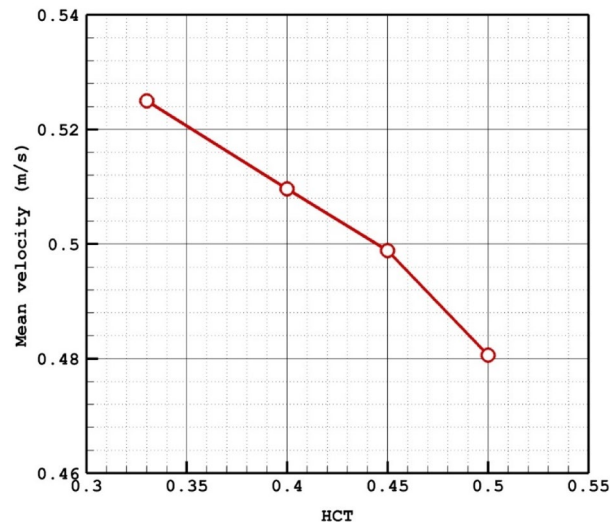


Figure 9. HCT effects on mean sac velocity.

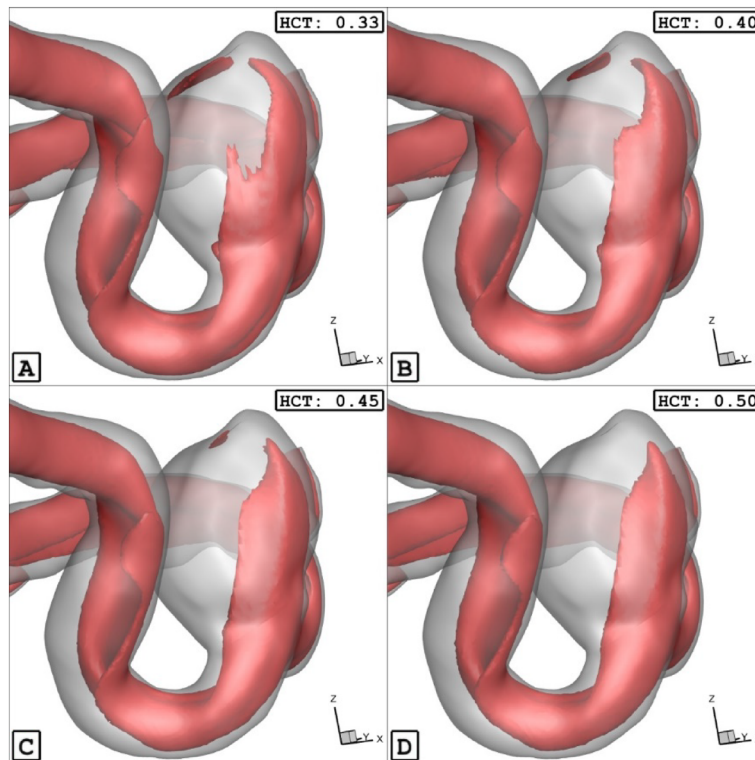


Figure 10. ISO surface velocity (1 m/sec) in different HCTs.

The Fig. 9 confirms that the increases of the HCT would result in lower mean velocity because of high viscosity. To notice the impacts of HCT, Fig. 10 illustrates the iso-velocity surface to compare the effects of the HCT on the blood hemodynamic inside the selected aneurysm at peak systolic instant. It is found that the HCT mainly impacts the blood feature inside the sac rather than the nearby wall.

Coiling Porosity effects. The coiling technique is recognized as the main technique for the treatment of the saccular aneurysm. Table 3 presents the results of blood flow features in different coiling porosities. Figure 11 plots the porosity impacts on mean values of WSS, OSI, sac pressure, and sac velocity at peak systolic instant on the selected aneurysm (D).

Permeability ($\text{m}^2 \times 10^{-8}$)	Porosity	WSS Max Sac (pa)	WSS Mean Sac (pa)	WSS Min Sac (pa)	OSI Max Sac	OSI Mean Sac	MWA_Vel_interior (m/s)	Sac mean pressure (pa)	Sac mean velocity (m/s)
1.54548	0.735	131.835	4.393409	0.237484	0.447007	0.03781	1.107858	19,940.34	0.2484077
2.47361	0.778	137.5839	5.648677	0.534482	0.432753	0.026943	1.102091	19,816.03	0.3160101
13.7441	0.892	151.3244	13.81179	0.208602	0.443797	0.020252	1.009931	19,490.09	0.4916839
144.47	0.964	207.534	18.37318	0.233454	0.404799	0.015257	0.990007	19,309.5	0.5270406

Table 3. Details of obtained results on selected model (D) for different coiling porosity.

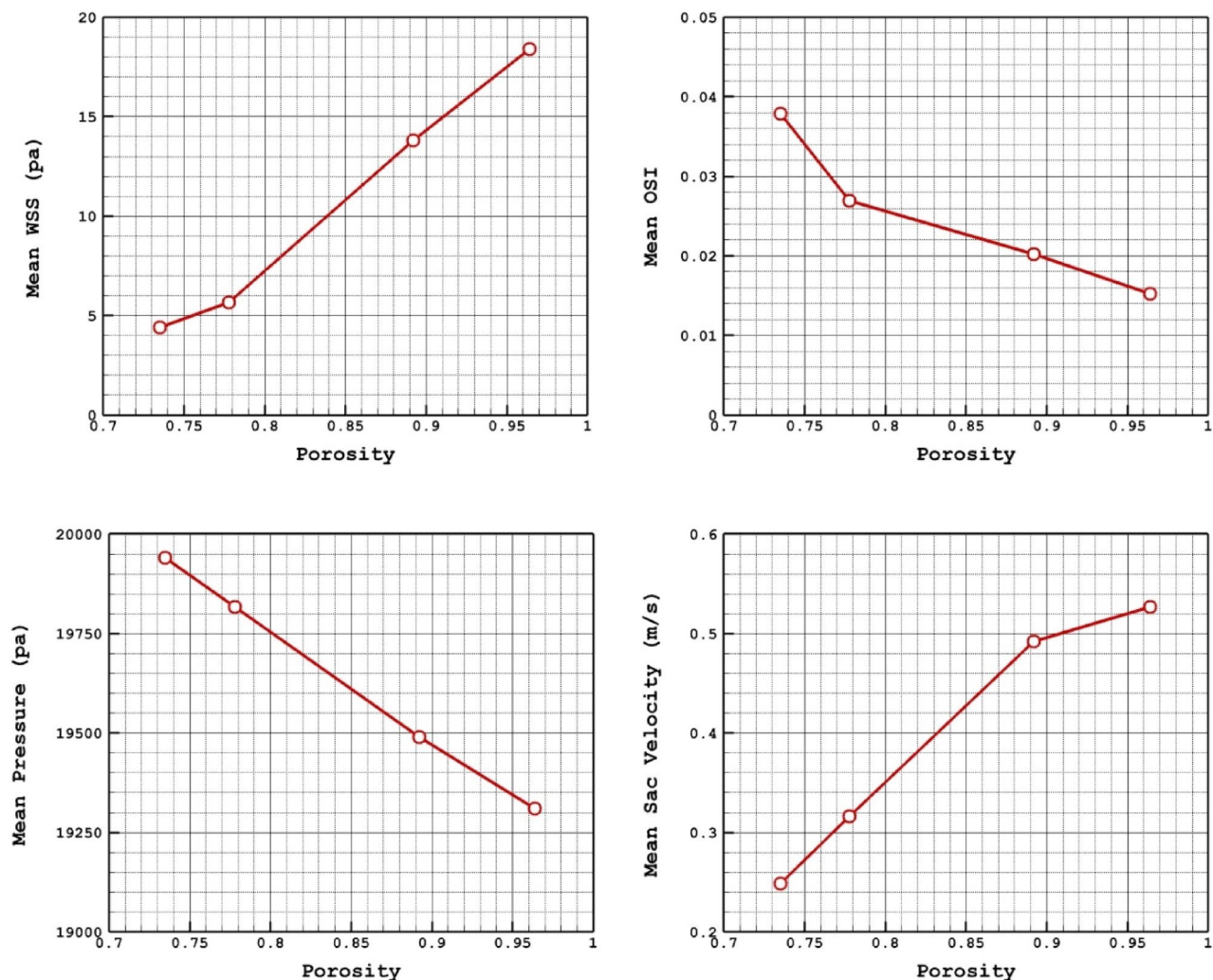


Figure 11. Porosity effects on mean values of WSS, OSI, sac pressure and sac velocity at peak systolic instant on the selected aneurysm (D).

The Fig. 12 displays the effect of porosity on the WSS distributions. It is found that the maximum WSS happens nearby the dome in low porosity. As the porosity of coiling increases, it happens near the sac neck. As presented in Fig. 11, the increase of the porosity would increase the mean WSS and sac velocity while it decreases mean pressure and OSI inside the aneurysm. Figure 13 also confirms the distribution of OSI on the sac wall for

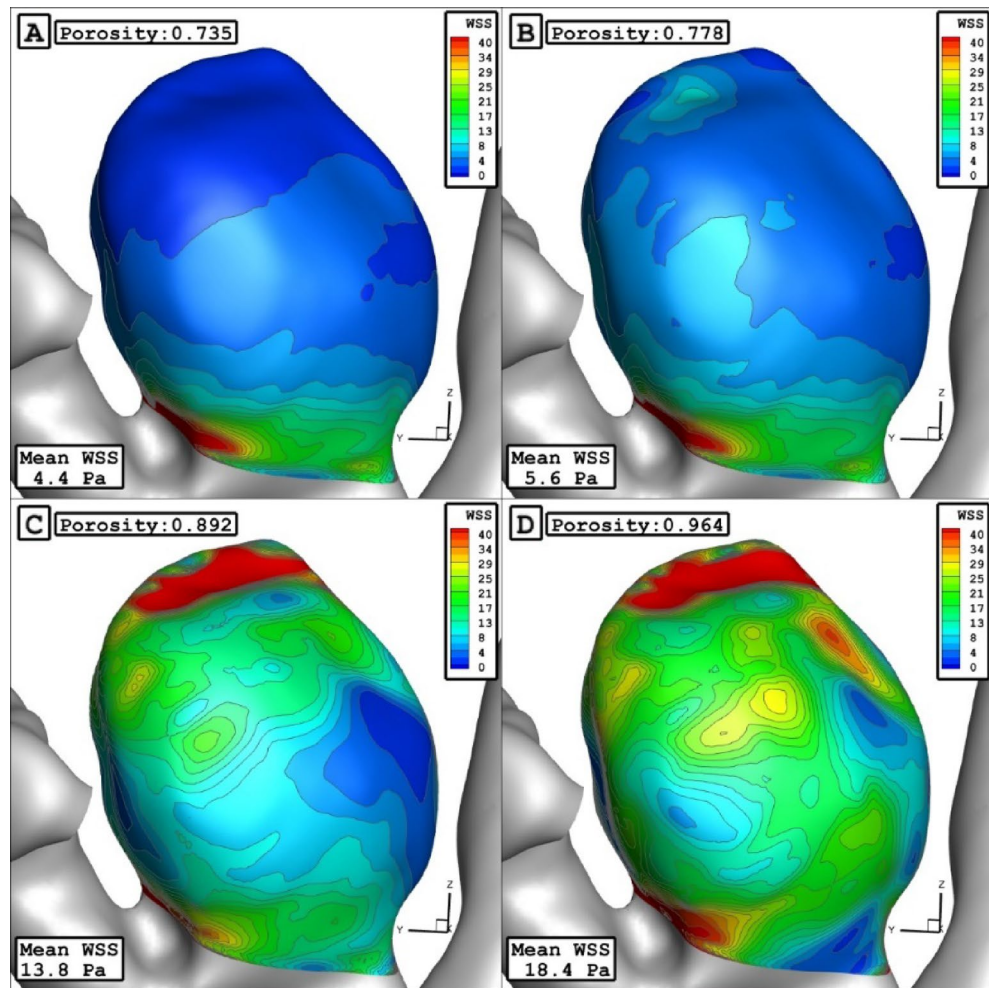


Figure 12. WSS contours in different porosities.

different coiling porosities. It is observed that the high value of the OSI occurs in the middle of the domain far from the neck and dome.

The Fig. 14 demonstrates the blood feature in presence of different coiling porosity. As noticed in the figure, the permeability of coiling decreases by increasing the coiling porosity. Therefore, the penetration of the blood stream inside the sac is limited as the porosity decreases inside the sac. As demonstrated in Fig. 15, the blood stream is highly limited when the permeability of coiling is increased (or porosity is decreased.)

Conclusion

This study conducts through computational analyses to uncover the influence of blood hemodynamics on six distinct saccular ICAs. Specifically, the study extensively explores the effects of the sac centerline, which is a key geometric characteristic of the saccular aneurysm. The study compares the primary parameters of wall shear stress (WSS), oscillatory shear index (OSI), pressure, and velocity among these models with varying sac centerlines. Our work tries to disclose the effect of blood HCT on the risk of aneurysm rupture in one specific aneurysm in peak systolic time instant. Blood stream and feature are also compared for various viscosity of the blood flow. In addition, the influence of the coiling porosity on rupture risk of the aneurysm is fully investigated in the present work. According to our findings, increasing the HCT would increase the WSS and pressure value on the aneurysm wall while OSI and mean velocity decreases by high value of blood HCTs. Our results also show that the coiling technique could sufficiently decrease the risk of rupture since decreasing the coil porosity (increasing the coil permeability) would increase the OSI and pressure and decrease WSS and blood velocity inside the sac. It is observed that the value of mean HCT decreases about 60% with 40% increase of HCT.

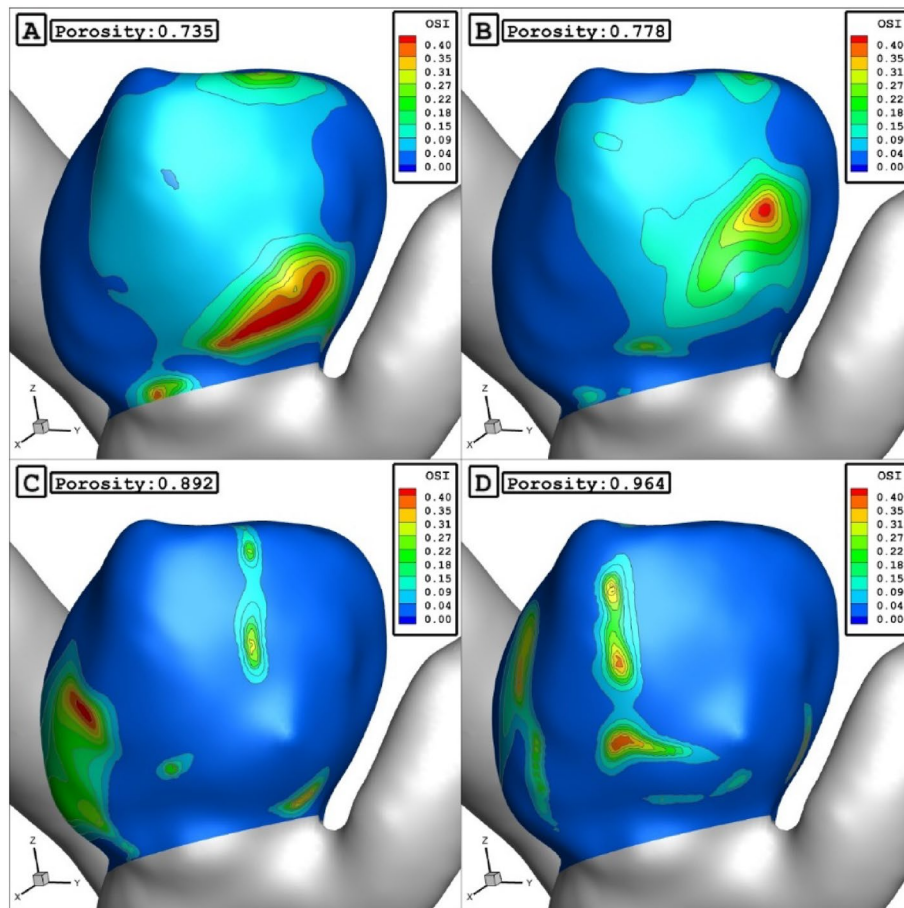


Figure 13. OSI contours in different porosities.

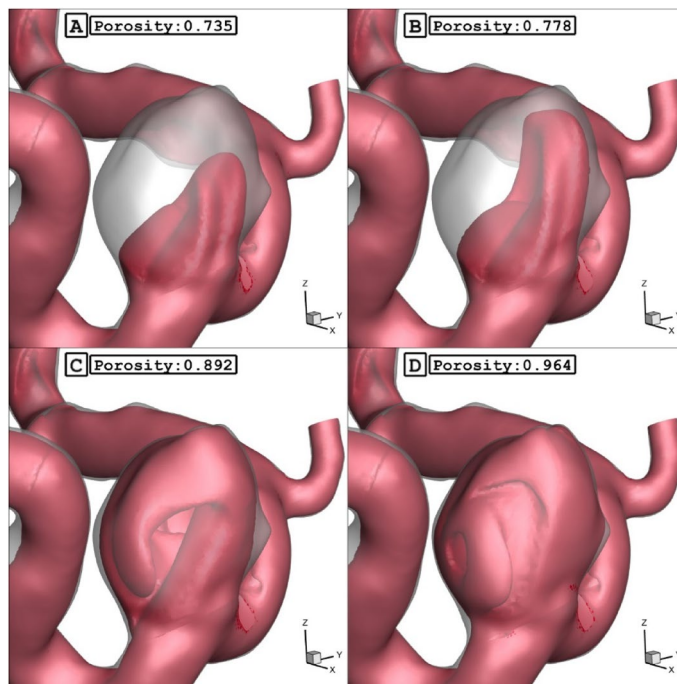


Figure 14. ISO surface velocity (0.3 m/sec) in different porosity.

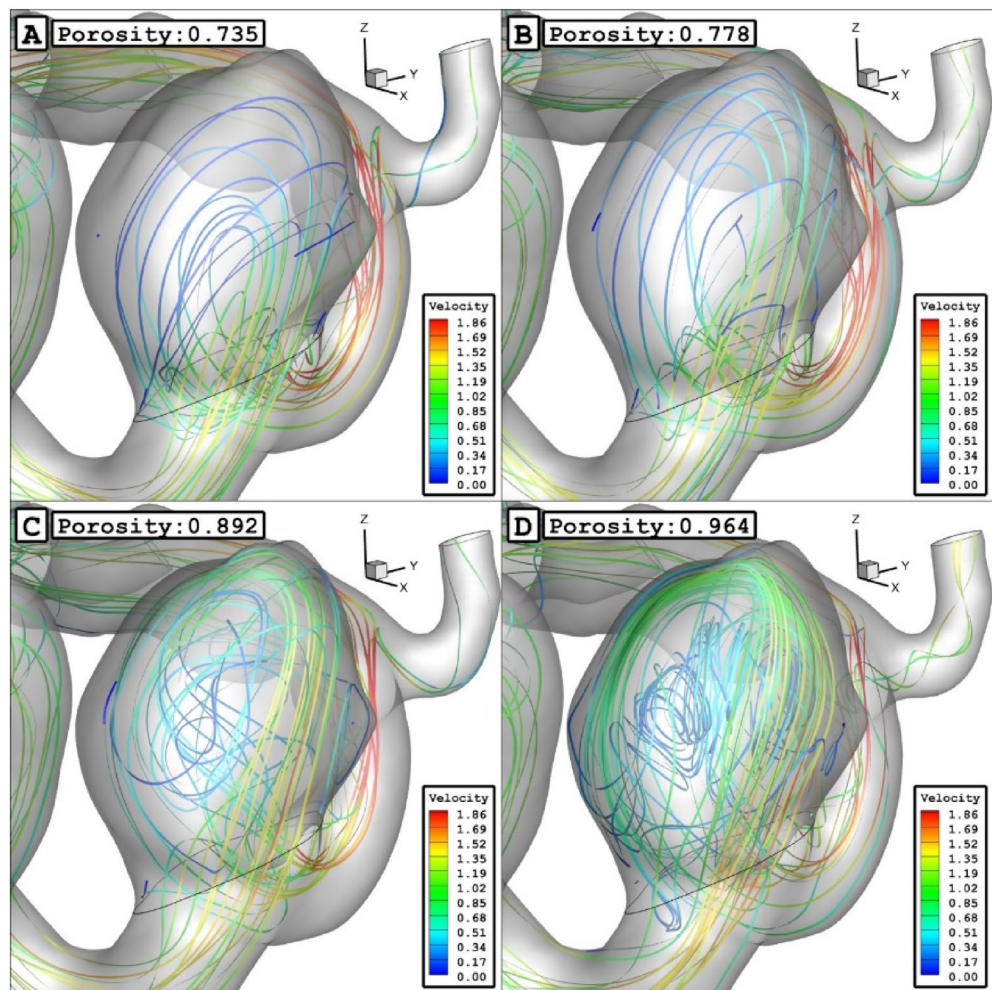


Figure 15. Streamlines in different porosity.

Data availability

All data generated or analysed during this study are included in this published article.

Received: 8 March 2023; Accepted: 8 July 2023

Published online: 12 July 2023

References

1. Sabernaemi, A. *et al.* Influence of stent-induced vessel deformation on hemodynamic feature of bloodstream inside ICA aneurysms. *Biomech. Model. Mechanobiol.* <https://doi.org/10.1007/s10237-023-01710-9> (2023).
2. Salavatidezfouli, S. *et al.* Investigation of the stent induced deformation on hemodynamic of internal carotid aneurysms by computational fluid dynamics. *Sci. Rep.* **13**, 7155 (2023).
3. Sheidani, A. *et al.* Influence of the coiling porosity on the risk reduction of the cerebral aneurysm rupture: Computational study. *Sci. Rep.* **12**, 19082 (2022).
4. Sadeh, A. *et al.* Computational study of blood flow inside MCA aneurysm with/without endovascular coiling. *Sci. Rep.* **13**, 4560. <https://doi.org/10.1038/s41598-023-31522-x> (2023).
5. Mirzaei Poueinak, M. *et al.* Computational study of blood hemodynamic in ICA aneurysm with coiling embolism. *Int. J. Mod. Phys. C* **465**, 2350138. <https://doi.org/10.1142/S0129183123501383> (2023).
6. Hariri, S., Poueinak, M. M., Hassanvand, A., Gerdroodbary, M. B. & Faraji, M. Effects of blood hematocrit on performance of endovascular coiling for treatment of middle cerebral artery (MCA) aneurysms: Computational study. *Interdiscip. Neurosurg.* **32**, 101729 (2023).
7. Jin, Z. H., Gerdroodbary, M. B., Valipour, P., Faraji, M. & Abu-Hamdeh, N. H. CFD investigations of the blood hemodynamic inside internal cerebral aneurysm (ICA) in the existence of coiling embolism. *Alex. Eng. J.* **66**, 797–809. <https://doi.org/10.1016/j.aej.2022.10.070> (2023).
8. Mousavi, S. J. *et al.* Coupling hemodynamics with mechanobiology in patient-specific computational models of ascending thoracic aortic aneurysms. *Comput. Methods Prog. Biomed.* **205**, 106107 (2021).
9. Nikonovas, T., Spessa, A., Doerr, S. H., Clay, G. D. & Mezbahuddin, S. Near-complete loss of fire-resistant primary tropical forest cover in Sumatra and Kalimantan. *Commun. Earth Environ.* **1**(1), 65 (2020).
10. Sadeh, A., Kazemi, A., Bahramkhoo, M. & Barzegar Gerdroodbary, M. Computational analysis of the blood hemodynamic inside internal cerebral aneurysm in the existence of endovascular coiling. *Int. J. Mod. Phys. C* **34**(05), 2350059 (2023).

11. Tateshima, S. *et al.* Three-dimensional blood flow analysis in a wide necked internal carotid artery-ophthalmic artery aneurysm. *J. Neurosurg.* **99**, 526–33 (2003).
12. Valipour, P. Effects of coiling embolism on blood hemodynamic of the MCA aneurysm: a numerical study. *Sci. Rep.* **12**(1), 22029 (2022).
13. Steinman, D. A., Milner, J. S., Norley, C. J., Lownie, S. P. & Holdsworth, D. W. Image-based computational simulation of flow dynamics in a giant intracranial aneurysm. *Am. J. Neuroradiol.* **24**, 559–566 (2003).
14. Chatziprodromou, I., Butty, V., Makhijani, V. B., Poulidakos, D. & Ventikos, Y. Pulsatile blood flow in anatomically accurate vessels with multiple aneurysms: A medical intervention planning application of computational haemodynamics. *Flow Turbul. Combust.* **71**, 333–346 (2003).
15. Shen, X. Y., Gerdroodbary, M. B., Abazari, A. M. & Moradi, R. Computational study of blood flow characteristics on formation of the aneurysm in internal carotid artery. *Eur. Phys. J. Plus* **136**(5), 541 (2021).
16. Shen, X. Y. *et al.* Numerical simulation of blood flow effects on rupture of aneurysm in middle cerebral artery. *Int. J. Mod. Phys. C* **33**(03), 2250030 (2022).
17. Fung, Y. C. *Biomechanics: Mechanical Properties of Living Tissues* 2nd edn. (Springer, 1993).
18. Razavi, A., Shirani, E. & Sadeghi, M. Numerical simulation of blood pulsatile flow in a stenosed carotid artery using different rheological models. *J. Biomech.* **44**, 2021–2030 (2011).
19. AneuriskWeb project website. Emory University, Department of Math & CS (2012), <http://ecm2.mathcs.emory.edu/aneuriskweb>.
20. Malvè, M. *et al.* Impedance-based outflow boundary conditions for human carotid haemodynamics. *Comput. Methods Biomech. Biomed. Engin.* **17**(11), 1248–1260 (2014).
21. Rostamian, A., Fallah, K., Rostamiyan, Y. & Alinejad, J. Application of computational fluid dynamics for detection of high risk region in middle cerebral artery (MCA) aneurysm. *Int. J. Mod. Phys. C* **34**(02), 2350019 (2023).
22. Dai, Z., Xie, J. & Jiang, M. A coupled peridynamics-smoothed particle hydrodynamics model for fracture analysis of fluid-structure interactions. *Ocean Eng.* **279**, 114582. <https://doi.org/10.1016/j.oceaneng.2023.114582> (2023).
23. Lu, L. *et al.* New insights into natural products that target the gut microbiota: Effects on the prevention and treatment of colorectal cancer. *Front. Pharmacol.* **13**, 964793. <https://doi.org/10.3389/fphar.2022.964793> (2022).
24. Lan, J. *et al.* Tumor-specific carrier-free nanodrugs with GSH depletion and enhanced ROS generation for endogenous synergistic anti-tumor by a chemotherapy-photodynamic therapy. *Chem. Eng. J.* **407**, 127212. <https://doi.org/10.1016/j.cej.2020.127212> (2021).
25. Qin, S. *et al.* Efficient parallel simulation of hemodynamics in patient-specific abdominal aorta with aneurysm. *Comput. Biol. Med.* **136**, 104652 (2021).
26. Xu, L., Liang, F., Zhao, B., Wan, J. & Liu, H. Influence of aging-induced flow waveform variation on hemodynamics in aneurysms present at the internal carotid artery: A computational model-based study. *Comput. Biol. Med.* **101**, 51–60 (2018).
27. Boccadifuoco, A., Mariotti, A., Celi, S., Martini, N. & Salvetti, M. V. Impact of uncertainties in outflow boundary conditions on the predictions of hemodynamic simulations of ascending thoracic aortic aneurysms. *Comput. Fluids* **165**, 96–115 (2018).
28. Mitsos, A. P., Kakalis, N. M., Ventikos, Y. P. & Byrne, J. V. Haemodynamic simulation of aneurysm coiling in an anatomically accurate computational fluid dynamics model. *Neuroradiology* **50**, 341–347 (2008).
29. Valencia, A., Morales, H., Rivera, R., Bravo, E. & Galvez, M. Blood flow dynamics in patient-specific cerebral aneurysm models: The relationship between wall shear stress and aneurysm area index. *Med. Eng. Phys.* **30**, 329–340 (2008).
30. Lu, S. *et al.* Analysis and design of surgical instrument localization algorithm. *CMES Comput. Model. Eng. Sci.* **137**(1), 669–685. <https://doi.org/10.32604/cmesci.2023.027417> (2023).
31. Yang, B. *et al.* Motion prediction for beating heart surgery with GRU. *Biomed. Signal Process. Control* **83**, 104641. <https://doi.org/10.1016/j.bspc.2023.104641> (2023).

Author contributions

S.S. and M.B.G. wrote the main manuscript text and A.S. prepared figures. H.J. and Zh.L. edit the manuscript and responded to reviewers comments. All authors reviewed the manuscript.

Competing interests

The authors declare no competing interests.

Additional information

Correspondence and requests for materials should be addressed to Z.L. or M.B.G.

Reprints and permissions information is available at www.nature.com/reprints.

Publisher's note Springer Nature remains neutral with regard to jurisdictional claims in published maps and institutional affiliations.



Open Access This article is licensed under a Creative Commons Attribution 4.0 International License, which permits use, sharing, adaptation, distribution and reproduction in any medium or format, as long as you give appropriate credit to the original author(s) and the source, provide a link to the Creative Commons licence, and indicate if changes were made. The images or other third party material in this article are included in the article's Creative Commons licence, unless indicated otherwise in a credit line to the material. If material is not included in the article's Creative Commons licence and your intended use is not permitted by statutory regulation or exceeds the permitted use, you will need to obtain permission directly from the copyright holder. To view a copy of this licence, visit <http://creativecommons.org/licenses/by/4.0/>.

© The Author(s) 2023